XRCC1 suppresses somatic hypermutation and promotes alternative nonhomologous end joining in *Igh* genes

Huseyin Saribasak,[1] Robert W. Maul,[1] Zheng Cao,[1] Rhonda L. McClure,[1] William Yang,[1] Daniel R. McNeill,[2] David M. Wilson III,[2] and Patricia J. Gearhart[1]

[1]Laboratory of Molecular Biology and Immunology, and [2]Laboratory of Molecular Gerontology, National Institute on Aging, National Institutes of Health, Baltimore, MD 21224

Activation-induced deaminase (AID) deaminates cytosine to uracil in immunoglobulin genes. Uracils in DNA can be recognized by uracil DNA glycosylase and abasic endonuclease to produce single-strand breaks. The breaks are repaired either faithfully by DNA base excision repair (BER) or mutagenically to produce somatic hypermutation (SHM) and class switch recombination (CSR). To unravel the interplay between repair and mutagenesis, we decreased the level of x-ray cross-complementing 1 (XRCC1), a scaffold protein involved in BER. Mice heterozygous for XRCC1 showed a significant increase in the frequencies of SHM in *Igh* variable regions in Peyer's patch cells, and of double-strand breaks in the switch regions during CSR. Although the frequency of CSR was normal in *Xrcc1*$^{+/-}$ splenic B cells, the length of microhomology at the switch junctions decreased, suggesting that XRCC1 also participates in alternative nonhomologous end joining. Furthermore, *Xrcc1*$^{+/-}$ B cells had reduced *Igh/c-myc* translocations during CSR, supporting a role for XRCC1 in microhomology-mediated joining. Our results imply that AID-induced single-strand breaks in *Igh* variable and switch regions become substrates simultaneously for BER and mutagenesis pathways.

CORRESPONDENCE
Patricia J. Gearhart:
gearhartp@mail.nih.gov

Abbreviations used: AID, activation-induced deaminase; A-NHEJ, alternative nonhomologous end joining; APE1, apurinic/apyrimidinic endonuclease 1; BER, base excision repair; ChIP, chromatin immunoprecipitation; C-NHEJ, classical NHEJ; CSR, class switch recombination; EdU, ethyl-2-deoxyuridine; LM-PCR, ligation-mediated PCR; MMS, methyl methanesulfonate; SHM, somatic hypermutation; UNG, uracil DNA glycosylase; XRCC1, x-ray cross-complementing 1.

In activated B cells, activation-induced deaminase (AID) deaminates cytosine in variable (V) and switch (S) regions to produce a U:G mismatch. Uracil DNA glycosylase (UNG) removes the rogue uracil to produce an abasic site, and apurinic/apyrimidinic endonuclease 1 (APE1) cleaves the abasic site to generate a single-strand break. The strand breaks can be processed either by proteins in the DNA base excision repair (BER) pathway to promote faithful DNA repair (Wilson and Bohr, 2007), or by proteins in a mutagenesis pathway to produce somatic hypermutation (SHM) and class switch recombination (CSR) for affinity maturation and isotype switching, respectively (Maul and Gearhart, 2010). In this paper, we define high-fidelity BER as the process that involves DNA synthesis by either polymerase β via a short-patch repair mechanism or polymerases δ or ε via a long-patch repair mechanism. The end process of BER is ligation of the single-strand break. Mutagenesis during SHM is defined as a low-fidelity type of BER that engages the error-prone polymerases, such as DNA polymerase η. Mutagenesis during CSR involves the joining of nearby single-strand breaks, which creates double-strand breaks, by a nonhomologous end joining pathway. The end process of mutagenesis is a high frequency of nucleotide substitutions (SHM) and DNA recombination (CSR). Therefore, the question arises as to whether BER and mutagenesis compete for the single-strand breaks in the *Igh* locus.

Because UNG and APE1 are used for the initial processing of the U:G pair, lack of these proteins should alter both repair and mutagenesis. In UNG-deficient mice and chicken DT40 cells, the mutation frequency in V_H and V_λ genes was somewhat higher compared with wild-type cells, suggesting that BER is compromised in the absence of UNG (Di Noia and Neuberger, 2002; Saribasak et al., 2006; Storb et al., 2009). However, UNG-deficient cells

The Rockefeller University Press $30.00
J. Exp. Med. Vol. 208 No. 11 2209-2216
www.jem.org/cgi/doi/10.1084/jem.20111135

also had an altered spectrum of substitutions, showing that UNG participates in mutagenesis (Rada et al., 2002; Saribasak et al., 2006; Rajagopal et al., 2009). Thus, UNG is required for both repairing mutations and generating them, which may explain why the mutation frequency was not dramatically increased in UNG-deficient mice. In addition, UNG-deficient mice had strikingly decreased CSR, implying that uracil excision precedes recombination (Rada et al., 2002). In mice with a haploinsufficiency of APE1, the frequency of double-strand breaks in the S_μ region and CSR was reduced (Guikema et al., 2007), indicating that APE1 also participates in both canonical BER and CSR. Therefore, the conundrum is why UNG and APE1 do not funnel all of the single-strand breaks into the high-fidelity BER pathway but leave some of them to become substrates for the mutagenesis pathway.

Another interpretation could be that UNG functions mainly in the mutagenesis pathway, and another uracil glycosylase, such as SMUG1, directs uracil repair into the faithful BER pathway (Di Noia et al., 2006). This is unlikely, however, because UNG is the most active uracil glycosylase in B cells, and the competition between repair and mutagenesis would mostly be for the single-strand breaks produced by APE1 incision of the abasic sites generated by UNG. In this regard, it should be noted that there will be breaks in the V region to allow entry for either DNA polymerase β to repair the break or DNA polymerase η and other low-fidelity polymerases to introduce nucleotide substitutions. DNA polymerases require a 3′ hydroxyl end to initiate synthesis, which could be provided by nicks from APE1 cleavage or from mismatch repair. Of course, single-strand breaks in the S regions are more abundant and easily detected as a result of the high frequency of AID hotspots and RNA pausing.

Another BER protein, DNA polymerase β, which replaces the excised nucleotide, was examined for its effect on SHM and CSR. In polymerase β–deficient B cells, the mutation frequency was increased in V and S regions, and there were more double-strand breaks in S regions and slightly increased CSR (Poltoratsky et al., 2007; Wu and Stavnezer, 2007). Therefore, polymerase β appears to function solely within the BER pathway to repair AID-induced strand breaks, and in its absence, SHM and CSR are elevated. The synthesized ends are then sealed by DNA ligase 3 to provide a corrected product. The role of this ligase in SHM and CSR can only be predicted because DNA ligase 3–deficient mice are not viable (Puebla-Osorio et al., 2006).

In this study, we examine the involvement of a scaffold protein in the BER pathway, x-ray cross-complementing 1 (XRCC1), in repairing AID-induced lesions. Although it has no enzymatic activity, XRCC1 interacts with DNA polymerase β and DNA ligase 3 to stabilize the proteins (Caldecott, 2003; Parsons et al., 2008). This suggests that a deficiency in XRCC1 would impair their function during BER, and increase the frequency of SHM and CSR. XRCC1 also interacts with PARP1 (Audebert et al., 2004), which may bind to the DNA breaks that are induced during CSR. Mice deficient in PARP1 had a normal frequency of

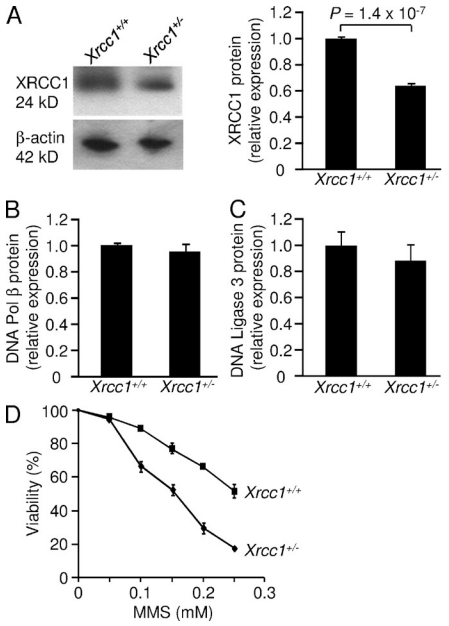

Figure 1. *Xrcc1*$^{+/-}$ cells have reduced levels of protein and are more sensitive to MMS damage. (A) Protein levels of XRCC1. Protein from lysates from resting B cells was measured by Western blot and is shown relative to β-actin. Error bars represent the SD of values from three independent experiments with one to two mice per genotype per experiment. Significance was determined by the student *t* test. (B) Protein levels for DNA polymerase β and (C) DNA ligase 3 in *Xrcc1*$^{+/+}$ and *Xrcc1*$^{+/-}$ B cells. Western blot analysis was performed on whole cell lysates from day-3 cells activated with LPS and IL-4 and are shown relative to β-actin levels. Error bars represent the SD of values from four independent experiments with two mice per genotype per experiment. (D) DNA repair after MMS damage. B cells were activated ex vivo, treated with MMS on day 1, and viability was measured by staining with propidium iodide on day 2. Error bars represent the SD of values from two independent experiments using two mice per genotype for one experiment and one mouse per genotype for another experiment.

CSR, but the S_μ-S_γ3 joins had less microhomology than joins from wild-type mice (Robert et al., 2009). Thus, PARP1, and possibly XRCC1, may function during CSR through alternative nonhomologous end joining (A-NHEJ), which is characterized by microhomology at the junctions, rather than through classical NHEJ (C-NHEJ), which produces mostly blunt joins. In addition, A-NHEJ has been shown to facilitate chromosomal translocations (Yan et al., 2007; Boboila et al., 2010a; Simsek and Jasin, 2010), implying that XRCC1 could affect the frequency of translocations. XRCC1 may, therefore, be a versatile player in both BER and A-NHEJ and have an effect on SHM, CSR, and translocations in B cells. Because XRCC1 is required for embryonic development (Tebbs et al., 1999), we used heterozygous mice to study its role in the frequencies of mutation in the V region, double-strand breaks in S_μ, CSR to various isotypes, microhomology at S_μ-S_γ3 joins, and translocations between *Igh* and *c-myc* loci.

A J_H4 region in Peyer's patch B cells

	4 month old		9 month old	
	Xrcc1$^{+/+}$	*Xrcc1*$^{+/-}$	*Xrcc1*$^{+/+}$	*Xrcc1*$^{+/-}$
Number of sequences	95	101	33	39
Mutated sequences	35	52	14	16
Bases in mutated sequences	16,707	24,001	6,888	7,872
Mutations	110	369	123	224
Mutations/base in mutated sequences	6.6×10^{-3}	15.4×10^{-3}	17.9×10^{-3}	28.5×10^{-3}

B

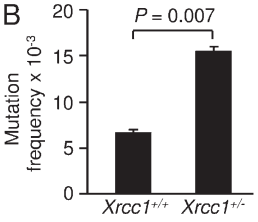

C

Xrcc1$^{+/+}$ (233 mutations)

From \ To	A	T	G	C	% Total
A	-	11	16	7	34
T	4	-	2	12	18
G	14	4	-	7	25
C	7	13	3	-	23

Xrcc1$^{+/-}$ (593 mutations)

From \ To	A	T	G	C	% Total
A	-	10	19	7	36
T	5	-	4	10	19
G	13	2	-	5	20
C	6	14	5	-	25

Figure 2. SHM analysis of *Xrcc1*$^{+/-}$ mice. Mutations in the J_H4 region of Peyer's patch B cells from *Xrcc1*$^{+/+}$ and *Xrcc1*$^{+/-}$ mice were identified by DNA sequencing. (A) For 4-mo mice, data are from two independent experiments with two mice per genotype per experiment, and for 9-mo mice, data are from one experiment with two mice per genotype. (B) Mean frequency (mutations/base) with SD from 4-mo-old mice. Significance was determined by the two-tailed student *t* test, comparing mutation frequencies from individual experiments. (C) Types of substitutions in *Xrcc1*$^{+/+}$ and *Xrcc1*$^{+/-}$ clones. The total number of mutations is shown in parentheses. Mutations were recorded from the nontranscribed strand and have been corrected for base composition of the nucleotide sequence. Data are expressed as percent of total mutations.

RESULTS AND DISCUSSION

Xrcc1$^{+/-}$ B cells have reduced BER

To ensure that XRCC1 is down-regulated in heterozygous mice, we measured RNA and protein levels in resting splenic B cells. Transcript levels were detected by quantitative PCR of cDNA, which was amplified with primers located downstream of the deleted exon 8 (Tebbs et al., 1999). There was a 38% reduction of XRCC1 transcripts in *Xrcc1*$^{+/-}$ cells compared with *Xrcc1*$^{+/+}$ cells (unpublished data). Protein levels were measured by Western blotting of whole cell extracts with antibody to XRCC1, and the results confirmed a 40% reduction in the heterozygous cells (Fig. 1 A; $P = 1.4 \times 10^{-7}$). Reduced XRCC1 protein could affect the stability of DNA polymerase β and DNA ligase 3. We determined the levels of these enzymes by western analyses and found that the amounts of DNA polymerase β (Fig. 1 B) and DNA ligase 3 (Fig. 1 C) were similar in both *Xrcc1*$^{+/+}$ and *Xrcc1*$^{+/-}$ B cells, indicating that the residual XRCC1 protein was sufficient to maintain stability of these two critical proteins. To determine if XRCC1 haploinsufficiency affected BER function, splenic B cells were activated with LPS plus IL-4 and incubated with various concentrations of methyl methanesulfonate (MMS), which leads to base loss and DNA strand breakage. As shown in Fig. 1 D, *Xrcc1*$^{+/-}$ cells were more sensitive to MMS compared with *Xrcc1*$^{+/+}$ cells, indicating that the physiological role of XRCC1 to repair breaks is impaired in these cells. Collectively, the reduced XRCC1 protein levels and lower repair activity suggest that the heterozygous mice are a good model to determine if high-fidelity BER competes with the mutagenesis pathway for access to DNA single-strand breaks.

Higher SHM frequency in V_H regions

SHM was detected in a 492-nucleotide region containing the intron downstream of rearranged J_H4 genes from germinal center–derived Peyer's patch B cells. The frequency of mutation was determined in 4-mo- and 9-mo-old littermate mice and is shown in Fig. 2 A. The frequency in mutated sequences from 4-mo-old mice was significantly higher (Fig. 2 B; $P = 0.007$) in *Xrcc1*$^{+/-}$ clones (15.4×10^{-3} mutations/base) than in *Xrcc1*$^{+/+}$ clones (6.6×10^{-3}).The frequency in 9-mo-old mice also was higher in *Xrcc1*$^{+/-}$ clones (28.5×10^{-3} mutations/base) compared with *Xrcc1*$^{+/+}$ clones (17.9×10^{-3}). The overall increase in mutations in older mice is in agreement with the study reporting that mutations accumulate with time in Peyer's patch B cells (González-Fernández et al., 1994). These results are striking because the haploinsufficient cells retained at least 50% of the protein. The types of mutations were similar between the two genotypes (Fig. 2 C), indicating that the increased mutations were generated by both the UNG and MSH2 pathways affecting G:C and A:T substitutions, respectively (Rada et al., 2004). Thus, the increased frequency of mutation was likely a result of inefficient repair in the heterozygous cells, because XRCC1 failed to adequately recruit DNA polymerase β and DNA ligase 3 to complete BER (Parsons et al., 2008). We propose that XRCC1 plays a role in promoting the accurate repair of single-strand breaks in V regions, and when the level of XRCC1 is reduced, more breaks are channeled into the mutagenesis pathway.

Increased double-strand breaks in S_μ

In the S_μ region, breaks are frequent as a result of multiple targeting sites for AID activity and prolonged RNA pausing in R-loops (Rajagopal et al., 2009; Wang et al., 2009). UNG and APE1 then produce single-strand breaks, which can be repaired by BER. Because XRCC1 is a major contributor to the repair of DNA single-strand breaks (Caldecott, 2003), it should be present in the S regions during CSR. We therefore measured the amount of protein at the S_μ region by chromatin immunoprecipitation (ChIP) analysis in ex vivo stimulated cells. Significantly higher levels of protein were detected bound to S_μ from *Xrcc1*$^{+/+}$ and *Xrcc1*$^{+/-}$ mice compared with *Aid*$^{-/-}$ mice ($P = 0.009$ and 0.038, respectively), and there was no increase in XRCC1 bound to the C_μ gene (Fig. 3 A). Thus, the heterozygous cells had a greater abundance of XRCC1 protein relative to AID-deficient cells, indicating that the protein is recruited to DNA breaks in S_μ. Single-strand

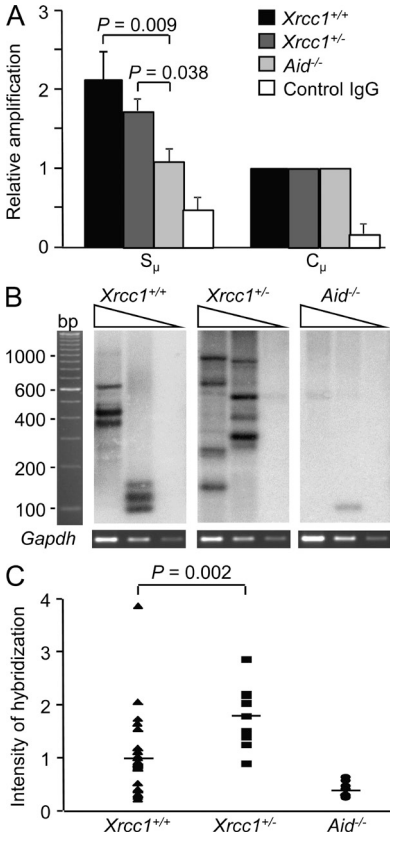

Figure 3. *Xrcc1*$^{+/-}$ cells have increased double-strand breaks. (A) Localization of XRCC1 to the S_μ region as assessed by ChIP in *Xrcc1*$^{+/+}$, *Xrcc1*$^{+/-}$, and *Aid*$^{-/-}$ cells stimulated with LPS and IL-4 for 2 d. Numbers are graphed relative to input DNA. Both S_μ and control IgG signals are standardized to C_μ signals. For *Xrcc1*$^{+/+}$ and *Aid*$^{-/-}$ cells, error bars represent the SD of values from three independent experiments with one mouse per genotype per experiment. For *Xrcc1*$^{+/-}$ cells, error bars represent the SD of values from two independent experiments with one mouse per genotype per experiment. Significance was determined by the Student's *t* test. (B) LM-PCR was performed on dilutions of DNA from cells stimulated with LPS plus IL-4, using *Gapdh* amplification as a loading control. After electrophoresis, bands were identified by hybridization to S_μ. Representative blots are shown. (C) Quantification of breaks from the LM-PCR assay was performed using the highest dilution of DNA and was calculated from 10 independent PCR reactions each from two *Xrcc1*$^{+/-}$ and two *Aid*$^{-/-}$ mice and 30 independent reactions from six *Xrcc1*$^{+/+}$ mice. Horizontal bars show the mean intensity of hybridization. Statistical analysis was performed using a two-tailed Student's *t* test.

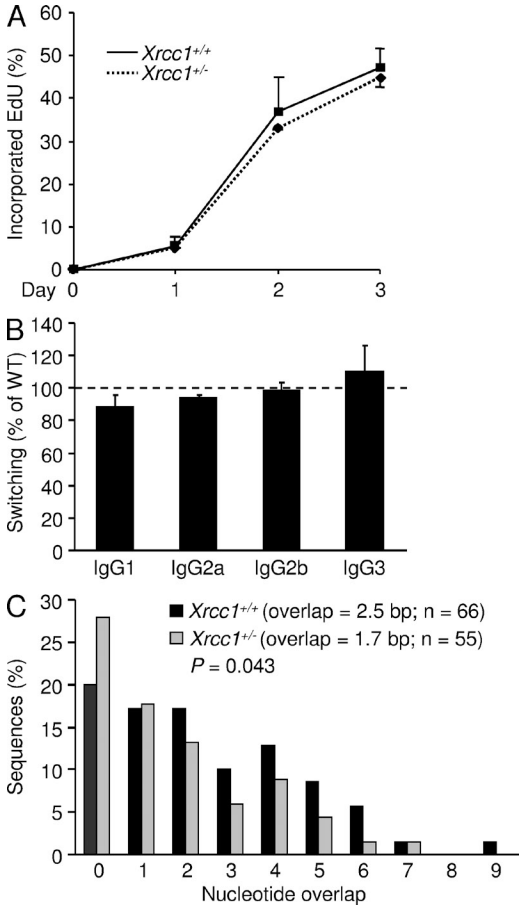

Figure 4. *Xrcc1*$^{+/-}$ cells have shorter overlaps in switch junctions. (A) DNA synthesis in *Xrcc1*$^{+/+}$ and *Xrcc1*$^{+/-}$ splenic B cells. Cells were cultured with LPS and IL-4 in the presence of EdU. Error bars represent the SD of values from two independent experiments with one mouse per genotype per experiment. (B) Percentage of switching to the indicated isotypes by *Xrcc1*$^{+/-}$ cells relative to *Xrcc1*$^{+/+}$ cells after 4 d in culture. Wild-type (WT) levels (dotted line) were 37% for IgG1, 17% for IgG2a, 32% for IgG2b, and 3% for IgG3. Error bars signify the SD of values from three independent experiments with two mice per genotype per experiment. (C) Microhomology in S_μ-$S_\gamma3$ switch joins from cells stimulated with LPS. Lengths of overlaps are depicted on the x-axis, and mean overlap for number (*n*) of sequences from two independent experiments with two mice per genotype per experiment is shown in the inset. Statistical difference was determined by the Mann-Whitney test.

breaks in close proximity on both strands can then be processed into double-strand breaks for recombination to downstream S regions. To measure the amount of double-strand breaks, a linker was ligated to DNA from cells stimulated for 2 d ex vivo, and the reactions were amplified by ligation-mediated PCR (LM-PCR) and separated by gel electrophoresis (Kong and Maizels, 2001; Guikema et al., 2007). Products containing S_μ DNA were identified by Southern hybridization, and representative blots are shown in Fig. 3 B. The bands represent breaks at different positions in S_μ, and the intensity of hybridization in each lane was quantified. *Xrcc1*$^{+/-}$ cells had significantly more breaks than *Xrcc1*$^{+/+}$ cells ($P = 0.002$), and *Aid*$^{-/-}$ cells had very few breaks (Fig. 3 C). These data indicate that XRCC1 plays a role in repairing AID-induced breaks in the S_μ region.

Similar frequency of CSR but shorter microhomology at switch junctions

The increased number of DNA breaks predicted that the frequency of CSR would be elevated. Before testing for CSR, we determined that *Xrcc1*$^{+/-}$ B cells underwent similar amounts of DNA synthesis as *Xrcc1*$^{+/+}$ spleen cells after stimulation with LPS and IL-4, as seen by incorporation of

ethyl-2-deoxyuridine (EdU), an analogue of thymidine (Fig. 4 A). Isotype switching was determined 4 d after addition of LPS plus various cytokines to induce switching from IgM to IgG1, IgG2a, IgG2b, or IgG3. There was no increase in the level of CSR to all isotypes (Fig. 4 B), even under suboptimal conditions of stimulation using less LPS and cytokines (Wu and Stavnezer, 2007; not depicted). Thus, despite the greater incidence of double-strand breaks, XRCC1 haploinsufficiency did not affect the overall frequency of CSR. Similar results were seen in DNA polymerase β–deficient cells, where increased double-strand breaks did not generate a corresponding increase in CSR (Wu and Stavnezer, 2007). In contrast, cells with decreased breaks as a result of reduced APE1 cleavage or altered switch regions still showed substantial recombination (Guikema et al., 2007; Zarrin et al., 2007). This indicates that only a few breaks can lead to recombination, and more breaks may not increase the frequency of CSR. Therefore, the frequency of switching does not accurately reflect the number of double-strand breaks.

Double-strand breaks in CSR are joined by either C-NHEJ, which is characterized by S-S joins with blunt or short overlapping nucleotides, or A-NHEJ, which generates joins with longer microhomologies. Experiments from several laboratories have demonstrated that in the absence of proteins that promote C-NHEJ, such as Ku, XRCC4, and DNA ligase 4, CSR occurs by A-NHEJ (Boboila et al., 2010b; Pan-Hammarström et al., 2005; Soulas-Sprauel et al., 2007; Yan et al., 2007). However, limited information is available about the proteins that are involved in A-NHEJ during CSR. PARP1 (Robert et al., 2009), MRN (Dinkelmann et al., 2009), Ku70 (Boboila et al., 2010b), and CtIP (Lee-Theilen et al., 2011) have recently been reported to play roles. Because XRCC1 has been shown to participate in A-NHEJ after DNA damage (Audebert et al., 2004; Wang et al., 2005), we reasoned that a reduction in XRCC1 would drive recombination toward the C-NHEJ route and produce S-S joins with more blunt joins and short overlaps. We sequenced S_μ-$S_\gamma 3$ junctions from spleen cells stimulated for 4 d with LPS (Fig. 4 C) because the length of $S_\gamma 3$ is shorter than other S regions, making it easier to identify homology after recombination. Microhomology was measured by the number of identical bases shared between S_μ and $S_\gamma 3$ at the break site (Fig. S1). There was a significant decrease in the mean length of microhomology in *Xrcc1*$^{+/-}$ cells (1.7 bp) compared with *Xrcc1*$^{+/+}$ cells (2.5 bp; P = 0.043), suggesting that XRCC1 is involved in A-NHEJ during CSR, likely through its interactions with PARP1 and DNA ligase 3.

XRCC1 facilitates *Igh/c-myc* translocations

AID-dependent chromosomal translocations between the oncogene *c-myc* and the S_μ region (Ramiro et al., 2004) are catalyzed by A-NHEJ (Boboila et al., 2010a). The data in the previous section shows that XRCC1 favored joining using longer microhomologies, which suggested that the protein has a role in generating translocations. To assess the frequency of translocations, we cultured splenic B cells from *Xrcc1*$^{+/+}$ and

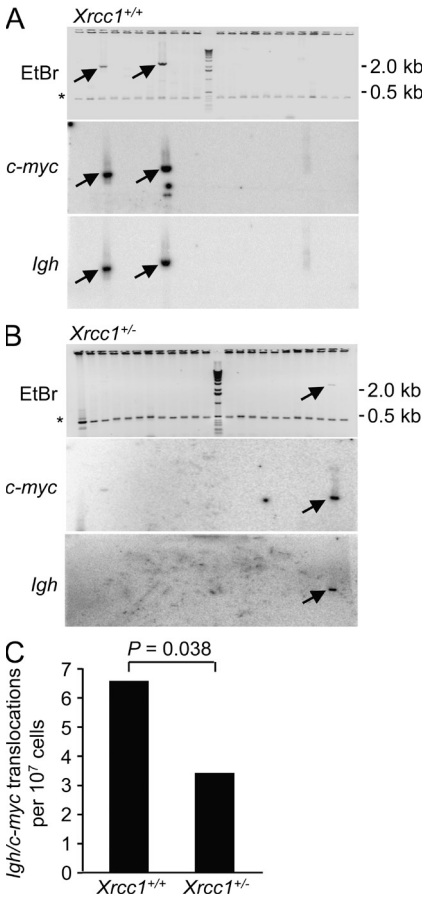

Figure 5. *Xrcc1*$^{+/-}$ cells have fewer *Igh/c-myc* translocations during CSR. (A) *Xrcc1*$^{+/+}$ and (B) *Xrcc1*$^{+/-}$ splenic B cells were analyzed for translocations. The top gels were stained with ethidium bromide (EtBr) and show the 484-bp *Aid* band (*), which was amplified as a loading control. The gels were then blotted and hybridized sequentially with *c-myc* and *Igh* (S_μ) probes. Representative blots are shown for chromosome 12. Arrows depict the bands that stained with both probes. (C) Frequency of translocations. P-values for pairwise comparison of translocation frequencies were calculated using the two-tailed Student's *t* test comparing the number of translocations per genotype (92 amplifications per mouse, three mice per genotype, 276 total amplifications).

Xrcc1$^{+/-}$ mice with LPS and IL-4 for 3 d. Translocations were measured by long-range PCR with both chromosome 12 and 15 primers and identified by Southern hybridization (Fig. 5, A and B). In amplifications from 2.7×10^7 cells per genotype, there were 18 translocations in *Xrcc1*$^{+/+}$ cells and 9 translocations in *Xrcc1*$^{+/-}$ cells. Therefore, the frequency in *Xrcc1*$^{+/+}$ cells was 6.5 translocations per 10^7 cells, in accord with a previously published study (Boboila et al., 2010a; Fig. 5 C). In *Xrcc1*$^{+/-}$ cells, there was a significant reduction in the frequency (3.4 per 10^7 cells; P = 0.038), suggesting that XRCC1 plays a role in the microhomology based pathway to promote chromosome translocations. Although a previous study (Robert et al., 2009) found no requirement for PARP1, a protein in A-NHEJ, in translocations during CSR, their conditions for stimulation in wild-type cells produced translocation frequencies of only 1.5 per 10^7 cells,

which would make it difficult to detect less frequent events. Thus, even though the frequency of recombination between S-S regions in *Xrcc1*$^{+/-}$ was normal, we have documented a decrease in recombination between S_μ and *c-myc*, perhaps because the latter is a rare event which reveals a quantitative difference.

BER is active in the *Ig* loci

BER resolves small base modifications, abasic sites, and single-strand breaks, all of which are abundant in V and S regions after AID is unleashed. The high frequency of mutations and seeming dearth of repair has been postulated to be a result of either a lack of faithful BER in the *Ig* loci or the very high level of damage induced by AID that could overwhelm BER. To what extent does BER compete with mutagenesis for DNA strand breaks? Our results show it is relatively easy to change the outcome by removing ∼40% of a BER scaffold protein, XRCC1, suggesting that alterations to the DNA synthesis and ligation steps of BER regulate the balance between accurate repair and mutagenesis. Our results confirm previous results showing increased mutations and double-strand breaks in B cells deficient for DNA polymerase β (Poltoratsky et al., 2007; Wu and Stavnezer, 2007), and they extend the SHM analysis for V regions undergoing mutation in vivo. The increase in SHM in BER-compromised cells implies that many AID-induced lesions are repaired faithfully by BER. The U:G mismatch is also recognized by proteins in the mismatch repair pathway, and a similar conclusion was reached for a balance between mismatch repair and mutagenesis in the *Ig* loci (Roa et al., 2010). Therefore, these data support an active role for DNA repair in V and S regions and favor the interpretation that the plethora of AID-induced damage allows some uracils to escape faithful repair and become substrates for the mutagenesis pathway.

MATERIALS AND METHODS

Mice. *Xrcc1*$^{+/-}$ mice on a C57BL/6 background were rederived from cryopreserved embryos as previously described (McNeill et al., 2011). Breeding pairs were set up as crosses between heterozygous and wild-type mice. Genotypes were confirmed by PCR of tail DNA using the primers listed in this section. To detect the *neo* cassette in exon 8 of the *Xrcc1* genomic locus, NEO-F01 (5′-GCTTGCCGAATATCATGGTG-3′) and TAR-D (5′-ATTAGGTTGGTGCCCCATCGAG-3′) generated a 450-bp band in heterozygous mice and no band in wild-type mice. To detect both targeting and wild-type alleles, TAR-C (5′-TGTCCTTCCATAGCCTCTACGAGTG-3′) and TAR-D generated a 441-bp band for wild-type and a 1597-bp band for the neomycin targeted allele. Littermate mice were used at 3–9 mo of age. *Aid*$^{-/-}$ mice on a C57BL/6 background were bred in our animal colony. All animal procedures were reviewed and approved by the Animal Care and Use Committee of the National Institute on Aging.

B cell isolation and ex vivo stimulation. Resting splenic B cells were isolated using negative selection with anti-CD43 and anti-CD11b magnetic beads (Miltenyi Biotec), according to the manufacturer's directions. Cells were plated at a density of 10^6 cells/ml if they were used on days 1–2, or 0.5×10^6 cells/ml if used on days 3–4. The cells were stimulated with 5 μg/ml *Escherichia coli* LPS serotype 0111:B4 (Sigma–Aldrich) and 5 ng/ml of recombinant mouse IL-4 (BD).

RNA and protein. RNA was isolated from resting cells using RNeasy Mini kit (QIAGEN), and qScript cDNA SuperMix was used to prepare cDNA (Quanta Biosciences). For quantitative real-time PCR, PerfeCTa SYBR Green FastMix was used (Quanta Biosciences) with the following primers: *β-actin* forward, 5′-GACCTCTATGCCAACACAGTGCTG-3′ and reverse, 5′-CACCGATCCACACAGAGTACTTGC-3′; and *Xrcc1* forward, 5′-AATGGCGAGGACCCGTATGC-3′ and reverse, 5′-CACGTAGCGGATGAGCCTCC-3′. Reactions were performed using a MyiQ real-time thermocycler (Bio-Rad Laboratories). Protein was isolated from B cells, and Western blotting was performed as previously described (McNeill et al., 2011) using antibodies directed against XRCC1 (gift from P. McKinnon, St. Jude Children's Research Hospital, New York, NY), DNA polymerase β (clone 18s; Abcam), and DNA ligase 3 (clone 7; BD).

DNA damage sensitivity. B cells were cultured with LPS and IL-4 for 24 h. The cells were centrifuged, and the media was saved for a second incubation. Cells were washed with phosphate-buffered saline, and 10^6 cells were treated for 1 h with concentrations of MMS (Sigma-Aldrich) indicated in Fig. 1 D. The cells were washed again, incubated in the original media for another 24 h, and viability was assessed by propidium iodide staining using flow cytometry.

SHM and microhomology. For SHM, cells from the Peyer's patches of 4- and 9-mo-old littermate mice were stained with phycoerythrin-labeled antibody to B220 (BD) and fluorescein-labeled peanut agglutinin (PNA; EY Laboratories). The $B220^+PNA^+$ population was isolated by cell sorting, and DNA was prepared. The 492-bp intronic region downstream of J_H4 from rearranged V_HJ558 genes was amplified using previously described forward and reverse primers (Martomo et al., 2005). Amplified DNA was then TA cloned into pGEM-T Easy vector (Promega) and clones were sequenced. Only unique mutations were recorded. For microhomology, splenic B cells were stimulated with LPS for 4 d, and DNA containing S_μ-$S_\gamma3$ joins was amplified and cloned as previously described (Wu and Stavnezer, 2007). Products ranged in size from 300 to 1,000 bp and were sequenced. The length of nucleotide overlap was based on perfect homology with no insertions.

DNA synthesis and ChIP. Splenic B cells were treated EdU (Invitrogen) according to the manufacturer's guidelines to measure DNA synthesis. Cells were incubated with LPS and IL-4 for 1–3 d and analyzed by flow cytometry. For ChIP assays, *Xrcc1*$^{+/+}$, *Xrcc1*$^{+/-}$, and *Aid*$^{-/-}$ splenic B cells were stimulated with LPS plus IL-4 for 2 d, and 10^7 cells were cross-linked with 1% formaldehyde at 37°C for 15 min. The reaction was quenched by adding glycine to a final concentration of 0.125 M at room temperature for 5 min. The cells were washed twice with 5 ml of cold phosphate-buffered saline supplemented with protease inhibitor cocktail tablet (Roche), lysed in 400 μl SDS lysis buffer (1% SDS, 10 mM EDTA, and 50 mM Tris-HCl, pH 8), and incubated on ice for 10 min. The reaction was then mixed with 600 μl ChIP dilution buffer (0.01% SDS, 1.1% Triton X-100, 1.2 mM EDTA, 16.7 mM Tris-HCl, pH 8, 16.7 mM NaCl, 1 mM PMSF, and protease inhibitor cocktail). Chromatin was sonicated to a mean length of ∼300 bp. Supernatant was saved and diluted fourfold in ChIP dilution buffer after centrifugation at 10,000 *g* for 30 min. One tenth of the diluted cell suspension was saved as input. To get rid of nonspecific IgG binding proteins, the remaining cell suspension was incubated with 36 μl Dynabeads Protein G (Invitrogen) and 5 μg of normal mouse IgG antibody (12–371; Millipore) at 4°C for 3 h. The suspension was then transferred into fresh 1.5-ml tubes and incubated with 36 μl Dynabeads Protein G and 5 μg rabbit anti-XRCC1 antibody (ab9147; Abcam) at 4°C for 16 h. DNA was washed and eluted, and the cross-links were reversed by heating the Dynabeads at 65°C for 5 h followed by protease K treatment at 45°C for 2 h. DNA was recovered by phenol:chloroform:isoamyl alcohol 25:24:1 (Sigma-Aldrich) extraction and ethanol precipitation. S_μ and C_μ sequences were quantified by quantitative PCR relative to input values. S_μ primers: forward, 5′-ACACTACTACATTCTTGATCTACAACTCAATGTGGT-3′, and reverse, 5′-CGGATCTAAGCACTGTCCTTTGATACCATTC-3′; C_μ primers: forward, 5′-TCTGACAGGAGGCAAGAAGACAGATTCTTA-3′, and reverse, 5′-GCCACCAGATTCTTATCAGACAGGGG-3′.

Double-strand break assay. Genomic DNA from 10^6 cells was isolated from cells stimulated with LPS plus IL-4 for 2 d, as previously described

(Guikema et al., 2007). DNA was digested in agarose plugs with proteinase K, washed, and equilibrated in 50 µl T4 ligase buffer. The agarose was melted, and 20 µl DNA was removed and mixed in a 60-µl reaction with a preannealed linker LL3/LP2 (Kong and Maizels, 2001) and T4 ligase for 16 h at 16°C. After ligation, samples were diluted fivefold in water and heated to 70°C for 10 min. To compare DNA recovery, threefold dilutions (spanning from 3- to 243-fold) were made and used as a template to amplify *Gapdh* as previously described (Maul et al., 2011). After standardization to *Gapdh*, double-strand breaks were amplified by nested PCR. The first round used forward primer LMPCR1 (5′-GAATTATTTCAGTTAAGTGTATTAGTTGAGGTACTGATGC-3′) and reverse primer LL4 (Kong and Maizels, 2001), and the second round used forward primer LMPCR2 (5′-GAATCTATTCTGGCTCTTCTTAAGCAG-3′) and reverse primer LL2 (Kong and Maizels, 2001). PCR products were separated by electrophoresis through a 1.2% agarose gel, blotted onto Hybond N^+ membrane (GE Healthcare), and hybridized with a ^{32}P-γATP labeled S_μ probe (5′-CTTACTGATTCTAAATTAGCTTCC-3′). The intensity of hybridization was quantified by exposure to a phosphorimager and analyzed using image quant software (GE Healthcare).

CSR. Resting splenic B cells from 3–4-mo-old littermate mice were stimulated with 5 µg/ml LPS for switching to IgG3, LPS plus 5 ng/ml IL-4 for switching to IgG1, LPS plus IL-4 plus 25 ng/ml IFN-γ (R&D Systems) and 0.5 µg/ml anti-CD40 (eBioscience) for switching to IgG2a, or LPS plus 2 ng/ml TGF-β (R&D Systems) and 0.5 µg/ml anti-CD40 for switching to IgG2b. After 4 d, the cells were stained with fluorescein-conjugated antibody to B220 (SouthernBiotech) and phycoerythrin-conjugated antibodies to mouse IgG1, IgG2a, IgG2b, or IgG3 (SouthernBiotech) for analysis by flow cytometry.

***Igh/c-myc* translocations.** DNA was collected from B cells stimulated with LPS and IL-4 for 3 d and resuspended at a ratio equivalent of 10^5 cells per µl. Nested PCR analysis of *Igh/c-myc* translocations on both chromosomes 12 and 15 was performed as previously described (Ramiro et al., 2004), and *Aid* was amplified as a positive control as previously described (Robert et al., 2009). 10 µl PCR products were separated by gel electrophoresis and stained with ethidium bromide. The gel was then blotted onto a Hybond N^+ membrane (GE Healthcare) and analyzed sequentially with *Igh* and *c-myc*–specific probes (Ramiro et al., 2004).

Online supplemental material. Fig. S1 lists the S_μ-S_γ3 joins with nucleotide overlaps for microhomology analysis. Online supplemental material is available at http://www.jem.org/cgi/content/full/jem.20111135/DC1.

We thank R. Wersto, C. Morris, J. Scheers, C. Nguyen, and T. Wolf for flow cytometry analyses, and Ranjan Sen and Sebastian Fugmann for valuable comments.

This research was supported entirely by the Intramural Research Program of the National Institutes of Health, National Institute on Aging.

The authors declare no competing financial interests.

Submitted: 6 June 2011
Accepted: 1 September 2011

REFERENCES

Audebert, M., B. Salles, and P. Calsou. 2004. Involvement of poly(ADP-ribose) polymerase-1 and XRCC1/DNA ligase III in an alternative route for DNA double-strand breaks rejoining. *J. Biol. Chem.* 279: 55117–55126. http://dx.doi.org/10.1074/jbc.M404524200

Boboila, C., M. Jankovic, C.T. Yan, J.H. Wang, D.R. Wesemann, T. Zhang, A. Fazeli, L. Feldman, A. Nussenzweig, M. Nussenzweig, and F.W. Alt. 2010a. Alternative end-joining catalyzes robust IgH locus deletions and translocations in the combined absence of ligase 4 and Ku70. *Proc. Natl. Acad. Sci. USA.* 107:3034–3039. http://dx.doi.org/10.1073/pnas.0915067107

Boboila, C., C. Yan, D.R. Wesemann, M. Jankovic, J.H. Wang, J. Manis, A. Nussenzweig, M. Nussenzweig, and F.W. Alt. 2010b. Alternative end-joining catalyzes class switch recombination in the absence of both Ku70 and DNA ligase 4. *J. Exp. Med.* 207:417–427. http://dx.doi.org/10.1084/jem.20092449

Caldecott, K.W. 2003. XRCC1 and DNA strand break repair. *DNA Repair* (*Amst.*). 2:955–969. http://dx.doi.org/10.1016/S1568-7864(03)00118-6

Di Noia, J., and M.S. Neuberger. 2002. Altering the pathway of immunoglobulin hypermutation by inhibiting uracil-DNA glycosylase. *Nature.* 419:43–48. http://dx.doi.org/10.1038/nature00981

Di Noia, J.M., C. Rada, and M.S. Neuberger. 2006. SMUG1 is able to excise uracil from immunoglobulin genes: insight into mutation versus repair. *EMBO J.* 25:585–595. http://dx.doi.org/10.1038/sj.emboj.7600939

Dinkelmann, M., E. Spehalski, T. Stoneham, J. Buis, Y. Wu, J.M. Sekiguchi, and D.O. Ferguson. 2009. Multiple functions of MRN in end-joining pathways during isotype class switching. *Nat. Struct. Mol. Biol.* 16:808–813. http://dx.doi.org/10.1038/nsmb.1639

González-Fernández, A., D. Gilmore, and C. Milstein. 1994. Age-related decrease in the proportion of germinal center B cells from mouse Peyer's patches is accompanied by an accumulation of somatic mutations in their immunoglobulin genes. *Eur. J. Immunol.* 24:2918–2921. http://dx.doi.org/10.1002/eji.1830241151

Guikema, J.E., E.K. Linehan, D. Tsuchimoto, Y. Nakabeppu, P.R. Strauss, J. Stavnezer, and C.E. Schrader. 2007. APE1- and APE2-dependent DNA breaks in immunoglobulin class switch recombination. *J. Exp. Med.* 204:3017–3026. http://dx.doi.org/10.1084/jem.20071289

Kong, Q., and N. Maizels. 2001. Breaksite batch mapping, a rapid method for assay and identification of DNA breaksites in mammalian cells. *Nucleic Acids Res.* 29:e33. http://dx.doi.org/10.1093/nar/29.6.e33

Lee-Theilen, M., A.J. Matthews, D. Kelly, S. Zheng, and J. Chaudhuri. 2011. CtIP promotes microhomology-mediated alternative end joining during class-switch recombination. *Nat. Struct. Mol. Biol.* 18:75–79. http://dx.doi.org/10.1038/nsmb.1942

Martomo, S.A., W.W. Yang, R.P. Wersto, T. Ohkumo, Y. Kondo, M. Yokoi, C. Masutani, F. Hanaoka, and P.J. Gearhart. 2005. Different mutation signatures in DNA polymerase eta- and MSH6-deficient mice suggest separate roles in antibody diversification. *Proc. Natl. Acad. Sci. USA.* 102:8656–8661. http://dx.doi.org/10.1073/pnas.0501852102

Maul, R.W., and P.J. Gearhart. 2010. AID and somatic hypermutation. *Adv. Immunol.* 105:159–191. http://dx.doi.org/10.1016/S0065-2776(10)05006-6

Maul, R.W., H. Saribasak, S.A. Martomo, R.L. McClure, W. Yang, A. Vaisman, H.S. Gramlich, D.G. Schatz, R. Woodgate, D.M. Wilson III, and P.J. Gearhart. 2011. Uracil residues dependent on the deaminase AID in immunoglobulin gene variable and switch regions. *Nat. Immunol.* 12:70–76. http://dx.doi.org/10.1038/ni.1970

McNeill, D.R., P.C. Lin, M.G. Miller, P.J. Pistell, N.C. de Souza-Pinto, K.W. Fishbein, R.G. Spencer, Y. Liu, C. Pettan-Brewer, W.C. Ladiges, and D.M. Wilson III. 2011. XRCC1 haploinsufficiency in mice has little effect on aging, but adversely modifies exposure-dependent susceptibility. *Nucleic Acids Res.* http://dx.doi.org/10.1093/nar/gkr280

Pan-Hammarström, Q., A.M. Jones, A. Lähdesmäki, W. Zhou, R.A. Gatti, L. Hammarström, A.R. Gennery, and M.R. Ehrenstein. 2005. Impact of DNA ligase IV on nonhomologous end joining pathways during class switch recombination in human cells. *J. Exp. Med.* 201:189–194. http://dx.doi.org/10.1084/jem.20040772

Parsons, J.L., P.S. Tait, D. Finch, I.I. Dianova, S.L. Allinson, and G.L. Dianov. 2008. CHIP-mediated degradation and DNA damage-dependent stabilization regulate base excision repair proteins. *Mol. Cell.* 29:477–487. http://dx.doi.org/10.1016/j.molcel.2007.12.027

Poltoratsky, V., R. Prasad, J.K. Horton, and S.H. Wilson. 2007. Down-regulation of DNA polymerase beta accompanies somatic hypermutation in human BL2 cell lines. *DNA Repair* (*Amst.*). 6:244–253. http://dx.doi.org/10.1016/j.dnarep.2006.10.003

Puebla-Osorio, N., D.B. Lacey, F.W. Alt, and C. Zhu. 2006. Early embryonic lethality due to targeted inactivation of DNA ligase III. *Mol. Cell. Biol.* 26:3935–3941. http://dx.doi.org/10.1128/MCB.26.10.3935-3941.2006

Rada, C., G.T. Williams, H. Nilsen, D.E. Barnes, T. Lindahl, and M.S. Neuberger. 2002. Immunoglobulin isotype switching is inhibited and

somatic hypermutation perturbed in UNG-deficient mice. *Curr. Biol.* 12:1748–1755. http://dx.doi.org/10.1016/S0960-9822(02)01215-0

Rada, C., J.M. Di Noia, and M.S. Neuberger. 2004. Mismatch recognition and uracil excision provide complementary paths to both Ig switching and the A/T-focused phase of somatic mutation. *Mol. Cell.* 16:163–171. http://dx.doi.org/10.1016/j.molcel.2004.10.011

Rajagopal, D., R.W. Maul, A. Ghosh, T. Chakraborty, A.A. Khamlichi, R. Sen, and P.J. Gearhart. 2009. Immunoglobulin switch mu sequence causes RNA polymerase II accumulation and reduces dA hypermutation. *J. Exp. Med.* 206:1237–1244. http://dx.doi.org/10.1084/jem.20082514

Ramiro, A.R., M. Jankovic, T. Eisenreich, S. Difilippantonio, S. Chen-Kiang, M. Muramatsu, T. Honjo, A. Nussenzweig, and M.C. Nussenzweig. 2004. AID is required for c-myc/IgH chromosome translocations in vivo. *Cell.* 118:431–438. http://dx.doi.org/10.1016/j.cell.2004.08.006

Roa, S., Z. Li, J.U. Peled, C. Zhao, W. Edelmann, and M.D. Scharff. 2010. MSH2/MSH6 complex promotes error-free repair of AID-induced dU:G mispairs as well as error-prone hypermutation of A:T sites. *PLoS ONE.* 5:e11182. http://dx.doi.org/10.1371/journal.pone.0011182

Robert, I., F. Dantzer, and B. Reina-San-Martin. 2009. Parp1 facilitates alternative NHEJ, whereas Parp2 suppresses IgH/c-myc translocations during immunoglobulin class switch recombination. *J. Exp. Med.* 206: 1047–1056. http://dx.doi.org/10.1084/jem.20082468

Saribasak, H., N.N. Saribasak, F.M. Ipek, J.W. Ellwart, H. Arakawa, and J.M. Buerstedde. 2006. Uracil DNA glycosylase disruption blocks Ig gene conversion and induces transition mutations. *J. Immunol.* 176:365–371.

Simsek, D., and M. Jasin. 2010. Alternative end-joining is suppressed by the canonical NHEJ component Xrcc4-ligase IV during chromosomal translocation formation. *Nat. Struct. Mol. Biol.* 17:410–416. http://dx.doi.org/10.1038/nsmb.1773

Soulas-Sprauel, P., G. Le Guyader, P. Rivera-Munoz, V. Abramowski, C. Olivier-Martin, C. Goujet-Zalc, P. Charneau, and J.P. de Villartay. 2007. Role for DNA repair factor XRCC4 in immunoglobulin class switch recombination. *J. Exp. Med.* 204:1717–1727. http://dx.doi.org/10.1084/jem.20070255

Storb, U., H.M. Shen, and D. Nicolae. 2009. Somatic hypermutation: processivity of the cytosine deaminase AID and error-free repair of the resulting uracils. *Cell Cycle.* 8:3097–3101. http://dx.doi.org/10.4161/cc.8.19.9658

Tebbs, R.S., M.L. Flannery, J.J. Meneses, A. Hartmann, J.D. Tucker, L.H. Thompson, J.E. Cleaver, and R.A. Pedersen. 1999. Requirement for the Xrcc1 DNA base excision repair gene during early mouse development. *Dev. Biol.* 208:513–529. http://dx.doi.org/10.1006/dbio.1999.9232

Wang, H., B. Rosidi, R. Perrault, M. Wang, L. Zhang, F. Windhofer, and G. Iliakis. 2005. DNA ligase III as a candidate component of backup pathways of nonhomologous end joining. *Cancer Res.* 65:4020–4030. http://dx.doi.org/10.1158/0008-5472.CAN-04-3055

Wang, L., R. Wuerffel, S. Feldman, A.A. Khamlichi, and A.L. Kenter. 2009. S region sequence, RNA polymerase II, and histone modifications create chromatin accessibility during class switch recombination. *J. Exp. Med.* 206:1817–1830. http://dx.doi.org/10.1084/jem.20081678

Wilson, D.M. III, and V.A. Bohr. 2007. The mechanics of base excision repair, and its relationship to aging and disease. *DNA Repair* (*Amst.*). 6:544–559. http://dx.doi.org/10.1016/j.dnarep.2006.10.017

Wu, X., and J. Stavnezer. 2007. DNA polymerase β is able to repair breaks in switch regions and plays an inhibitory role during immunoglobulin class switch recombination. *J. Exp. Med.* 204:1677–1689. http://dx.doi.org/10.1084/jem.20070756

Yan, C.T., C. Boboila, E.K. Souza, S. Franco, T.R. Hickernell, M. Murphy, S. Gumaste, M. Geyer, A.A. Zarrin, J.P. Manis, et al. 2007. IgH class switching and translocations use a robust non-classical end-joining pathway. *Nature.* 449:478–482. http://dx.doi.org/10.1038/nature06020

Zarrin, A.A., C. Del Vecchio, E. Tseng, M. Gleason, P. Zarin, M. Tian, and F.W. Alt. 2007. Antibody class switching mediated by yeast endonuclease-generated DNA breaks. *Science.* 315:377–381. http://dx.doi.org/10.1126/science.1136386